Scattering and fusion of identical heavy ions with arbitrary spin

A. J. Toubiana,[1,2,*] L. F. Canto,[3,4,†] R. Donangelo,[5,‡] and M. S. Hussein[6,7,8,§]

[1]*Departamento de Engenharia Nuclear, Escola Politécnica, Universidade Federal do Rio de Janeiro, C.P. 68529, 21941-909, Rio de Janeiro, RJ, Brazil*

[2]*École CentraleSupélec, Bâtiment Eiffel, 8-10 rue Joliot-Curie 91 190 Gif-sur-Yvette France*

[3]*Instituto de Física, Universidade Federal do Rio de Janeiro, CP 68528, 21941-972, Rio de Janeiro, RJ, Brazil*

[4]*Instituto de Física, Universidade Federal Fluminense, Av. Litoranea s/n, Gragoatá, Niterói, R.J., 24210-340, Brazil*

[5]*Instituto de Física, Facultad de Ingeniería, Universidad de la República, C.C. 30, 11000 Montevideo, Uruguay*

[6]*Departamento de Física Matemática, Instituto de Física, Universidade de São Paulo, C.P. 66318, 05314-970, São Paulo, SP, Brazil*

[7]*Instituto de Estudos Avançados, Universidade de São Paulo, C.P. 72012, 05508-970, São Paulo, SP, Brazil*

[8]*Departamento de Física, Instituto Tecnológico de Aeronáutica, CTA, São José dos Campos, São Paulo, SP, Brazil*

(Received 31 October 2017; published 22 December 2017)

The cross sections of elastic scattering and fusion of identical heavy ions with arbitrary spin, s are derived. Applications to several light heavy ions at near-barrier energies are made. It is found that the transverse isotropy; namely, the flat angular distribution which sets in at a critical value of the energy, becomes less pronounced with higher values of the spin. The oscillations in energy in the fusion cross section was found to go as $1/(2s+1)$. A similar factor is found in the angle-oscillating term in the elastic-scattering cross section.

DOI: 10.1103/PhysRevC.96.064615

I. INTRODUCTION

In this paper we develop the theory of elastic scattering and fusion of identical nuclei with arbitrary spin s. Although this topic is an old one, a systematic development for any value of spin of the participating nuclei is lacking in the literature. With respect to elastic scattering, we generalize our findings [1,2], discussing the transverse isotropy (TI) for nuclei with spin larger than zero and analyze the use of this phenomenon to discern the nuclear interaction at distances corresponding to energies slightly above the Coulomb barrier. In the case of fusion, we derive an expression for the cross section which clearly shows how the spin of the nucleus appears in the identity-related oscillatory term in the energy variation. We apply our findings to several light ion systems.

The paper is organized as follows: In Sec. II we give a short account of the wave function describing the scattering system. In Sec. III we derive the elastic-scattering cross section and show that the interference term, which expresses the coherence in the system, goes as $1/(2s+1)$, and accordingly for high values of s the cross section becomes the incoherent sum of the direct and the exchange contribution. We then discuss the origin of transverse isotropy (TI) and investigate this phenomenon in ^{6}Li-^{6}Li and ^{10}B-^{10}B collisions. These are the lightest systems of identical nuclei with integer spin, following ^{4}He + ^{4}He, where TI has been observed [2,3]. In Sec. IV the fusion cross section is derived, and its dependence on energy is analyzed. Both exact optical model calculations and approximate analytical calculations are presented for a few light systems of identical nuclei. Again we found that the oscillatory term depends on spin as $1/(2s+1)$. Finally, in Sec. V we present our concluding remarks. At the end of the paper we present two Appendixes: the first is meant to clarify the derivation of the general expression for the fusion cross section for identical nuclei with arbitrary spin, and the second supplies the details of the analytical calculation presented in Sec. IV.

II. SCATTERING WAVE FUNCTION IN COLLISIONS OF IDENTICAL PARTICLES

We consider the collision of two structureless identical particles, each with mass m, charge Ze, and intrinsic spin s, assuming that there is no spin flip. The properly symmetrized scattering wave function reads

$$\Psi^{(+)}_{\mu_1\mu_2}(\mathbf{r}) = \frac{1}{\sqrt{2}}[\psi(\mathbf{r})|s\mu_1 s\mu_2\rangle + (-)^{2s}\psi(-\mathbf{r})|s\mu_2 s\mu_1\rangle], \tag{1}$$

where μ_1, μ_2 are the z components of the spin of the two particles. The factor $(-)^{2s}$ guarantees the correct symmetry of the wave function with respect to exchange. It is equal to 1 in collisions of bosons and equal to (-1) in collisions of fermions. The function $\psi(-\mathbf{r})$ can be written in terms of the space reflection operator $\mathbb{P}$ as

$$\psi(-\mathbf{r}) = \mathbb{P}\psi(\mathbf{r}). \tag{2}$$

Equation (1) then becomes

$$\Psi^{(+)}_{\mu_1\mu_2}(\mathbf{r}) = \frac{1}{\sqrt{2}}[\psi(\mathbf{r})|s\mu_1 s\mu_2\rangle + (-)^{2s}\mathbb{P}\psi(\mathbf{r})|s\mu_2 s\mu_1\rangle]. \tag{3}$$

*ajtoubiana@gmail.com
†canto@if.ufrj.br
‡rdonangelo@gmail.com
§hussein@if.usp.br

It is convenient to express the spin state in the coupled basis, which has well-defined exchange properties, by writing

$$|s\mu_1 s\mu_2\rangle = \sum_{S=0}^{2s} \sum_{\nu=-S}^{S} \langle S\nu|s\mu_1 s\mu_2\rangle |S\nu\rangle \tag{4}$$

and

$$|s\mu_2 s\mu_1\rangle = \sum_{S=0}^{2s} \sum_{\nu=-S}^{S} \langle S\nu|s\mu_2 s\mu_1\rangle |S\nu\rangle. \tag{5}$$

Using the property (see p. 35 of Ref. [4])

$$\langle S\nu|s\mu_2 s\mu_1\rangle = (-)^{S-2s}\langle S\nu|s\mu_1 s\mu_2\rangle, \tag{6}$$

one gets

$$|s\mu_2 s\mu_1\rangle = \sum_{S=0}^{2s} (-)^{S-2s} \sum_{\nu=-S}^{S} \langle S\nu|s\mu_1 s\mu_2\rangle |S\nu\rangle. \tag{7}$$

Then, inserting Eqs. (5) and (7) in Eq. (1), one obtains

$$\Psi^{(+)}_{\mu_1\mu_2}(\mathbf{r}) = \frac{1}{\sqrt{2}} \sum_{S=0}^{2s} \sum_{\nu=-S}^{S} [\{1 + (-)^S \mathbb{P}\}\psi(\mathbf{r})] \times \langle S\nu|s\mu_1 s\mu_2\rangle |S\nu\rangle. \tag{8}$$

III. THE ELASTIC CROSS SECTION

To evaluate the differential elastic cross section for a CM collision energy E, one writes $\psi(\mathbf{r})$ as the sum of the incident (ϕ^{in}) and the scattered (ψ^{sc}) waves and takes the asymptotic form of the latter:

$$\psi^{\text{sc}}(\mathbf{r}) \longrightarrow A \frac{1}{\sqrt{2}} f(\theta) \frac{e^{i[kr - \eta \ln(kr)]}}{r}. \tag{9}$$

Above,

$$k = \frac{\sqrt{mE}}{\hbar} \tag{10}$$

is the wave number,

$$\eta = \frac{mZ^2e^2}{2\hbar^2 k} \tag{11}$$

is the Sommerfeld parameter, θ is the deflection angle, and A is a normalization constant. The factor within square brackets represents the asymptotic distortion of the outgoing spherical wave caused by the Coulomb field. Inserting Eq. (9) into Eq. (8), one obtains the asymptotic form of the scattered wave in the full (coordinate + spin) space. It can be put in the form

$$\Psi^{\text{sc}}_{\mu_1\mu_2}(\mathbf{r}) \longrightarrow A \frac{1}{\sqrt{2}} F_{\mu_1\mu_2}(\theta) \frac{e^{i[kr - \eta \ln(kr)]}}{r}, \tag{12}$$

with

$$F_{\mu_1\mu_2}(\theta) = \sum_{S=0}^{2s} \sum_{\nu=-S}^{S} [f(\theta) + (-)^S f(\pi - \theta)] \times \langle S\nu|s\mu_1 s\mu_2\rangle |S\nu\rangle. \tag{13}$$

The differential elastic cross section in a fully polarized collision where the z components of the spins of the collision partners are μ_1 and μ_2 is then given by

$$\sigma_{\mu_1\mu_2}(\theta) = 2F^{\dagger}_{\mu_1\mu_2}(\theta) F_{\mu_1\mu_2}(\theta). \tag{14}$$

The factor 2 accounts for the detection of both the projectile and the target nuclei, because they are identical [5].

The cross section in an unpolarized experiment is obtained summing over final spin states and taking the average over the $(2s+1)^2$ possible initial spin states. That is

$$\sigma(\theta) = \frac{1}{(2s+1)^2} \sum_{\mu_1\mu_2} \sigma_{\mu_1\mu_2}(\theta). \tag{15}$$

Inserting Eq. (13) into Eq. (14) and using the orthonormality of the spin states and a symmetry property of Clebsch–Gordan coefficients, one obtains

$$\sigma(\theta) = \frac{1}{(2s+1)^2} \sum_{S=0}^{2s} (2S+1)|f(\theta) + (-)^S f(\pi - \theta)|^2, \tag{16}$$

or

$$\sigma(\theta) = \frac{N_+ + N_-}{(2s+1)^2}[|f(\theta)|^2 + |f(\pi-\theta)|^2] + 2\frac{N_+ - N_-}{(2s+1)^2}\text{Re}\{f^*(\theta) f(\pi - \theta)\}. \tag{17}$$

Above, N_+ and N_- are respectively the numbers of even and odd values of S in the range $[0, 2s]$. These numbers are given below, for collisions of boson and for collisions fermion.

(1) *bosons* ($2s$ = even):

$$N_+ = \sum_{p=0}^{s} (4p+1) = (s+1)(2s+1), \tag{18}$$

$$N_- = \sum_{p=0}^{s-1} (4p+3) = s(2s+1). \tag{19}$$

(2) *fermions*:

$$N_+ = \sum_{p=0}^{s-1/2} (4p+1) = s(2s+1), \tag{20}$$

$$N_- = \sum_{p=0}^{s-1/2} (4p+3) = (s+1)(2s+1). \tag{21}$$

Using these results, one immediately gets

$$\frac{N_+ + N_-}{(2s+1)^2} = 1 \quad \text{and} \quad \frac{N_+ - N_-}{(2s+1)^2} = \frac{(-)^{2s}}{2s+1}. \tag{22}$$

Then, Eq. (17) can be put in the form

$$\sigma(\theta) = \sigma_{\text{inc}}(\theta) + \delta_{\text{int}}(\theta). \tag{23}$$

The first term in the above equation is

$$\sigma_{\text{inc}}(\theta) = |f(\theta)|^2 + |f(\pi - \theta)|^2. \tag{24}$$

It corresponds to the incoherent sum of the cross sections for detecting the projectile and for detecting the target. The second

term in Eq. (17) represents the interference of the scattering amplitudes for these processes. It is given by

$$\delta_{\rm int}(\theta) = 2\frac{(-)^{2s}}{2s+1}{\rm Re}\{f^*(\theta)f(\pi-\theta)\}. \quad (25)$$

Note that $\delta_{\rm int}(\theta)$ can take both positive and negative values. It represents the quantum mechanical correction to the incoherent cross section, giving the interference of the direct and exchange amplitudes.

A. Transverse isotropy: Mott-scattering case

Inspecting Eqs. (23)–(25), one concludes that the elastic cross section is symmetric with respect to $\theta = \pi/2$. Since this cross section is a continuous function of θ, its derivative at $\theta = \pi/2$ must vanish. Therefore, the elastic cross section will have a maximum or a minimum at $\pi/2$. This leads to the following question: What are the conditions for the cross section to have a maximum or to have a minimum at $\theta = \pi/2$? This question has been answered in the case of Mott scattering [1,2], as explained below.

In a typical nucleus-nucleus collision the scattering amplitude is given by

$$f(\theta) = f_{\rm C}(\theta) + f_{\rm N}(\theta), \quad (26)$$

where $f_{\rm C}(\theta)$ is the Coulomb amplitude and $f_{\rm N}(\theta)$ is a correction arising from the short-range nuclear potential. However, at energies well below the Coulomb barrier the influence of nuclear forces is negligible. Then, one can approximate in Eqs. (23)–(25) $f(\theta)$ by $f_{\rm C}(\theta)$. This process is known as Mott scattering and the elastic cross section in this case is known analytically. In Ref. [1] it was shown that $\sigma_{\rm inc}(\theta)$ and $\delta_{\rm int}(\theta)$ have opposite trends at $\theta = \pi/2$ and the behavior of the cross section near this angle is determined by a competition of the two. In the case of fermions, it was shown in Ref. [1] that the second derivative of the elastic differential cross section is always positive at $\theta = \pi/2$, therefore it is always a minimum. In the case of bosons, the result depends exclusively on the Sommerfeld parameter η. For large values of η (low collision energies) the Mott cross section has a maximum, whereas for small Sommerfeld parameters (high energies) it has a minimum. The transition between these two behaviors takes place at the critical value of the Sommerfeld parameter

$$\eta_{\rm C} = \sqrt{3s+2}. \quad (27)$$

For light bosonic systems, where $Z = A/2$, with A being the mass number of the colliding nuclei, this condition can be written as

$$E_{\rm C} = \frac{Z^5}{2\eta_{\rm C}^2}\left(\frac{e^2}{\hbar c}\right)^2 m_0c^2 = 0.025\left[\frac{Z^5}{3s+2}\right]{\rm MeV}. \quad (28)$$

The Mott differential cross section for bosonic systems exhibits a very unusual behavior at the energy $E_{\rm C}$: it is nearly constant over a broad angular region around $\pi/2$. The reason for this behavior, which was called *transverse isotropy* (TI) [1,2], is that both the first and the second derivatives of the Mott cross section with respect to θ vanish at $\pi/2$. Thus the first nonvanishing term in the Taylor expansion around $\pi/2$ is of fourth order.

TABLE I. TI energies and barrier heights for the first few light stable bosonic systems. The barrier heights $V_{\rm B}$ were determined by employing the Akyüz–Winther potential parametrization [6].

System	Spin	$E_{\rm C}$ (MeV)	$V_{\rm B}$ (MeV)	$E_{\rm M}/V_{\rm B}$
^{4}He + ^{4}He	0	0.40	0.87	0.46
^{6}Li + ^{6}Li	1	1.22	1.74	0.70
^{10}B + ^{10}B	3	7.05	4.40	1.61

B. Transverse isotropy: General case

A detailed investigation of TI in ^{4}He + ^{4}He scattering was carried out in Ref. [2]. In this case, the TI energy in Mott scattering is $E_{\rm C} = 0.40$ MeV. The fact that Mott scattering completely neglects nuclear effects is not expected to be a serious problem. Since the Coulomb barrier for this system is $V_{\rm B} \sim 0.8$ MeV, TI occurs well below the Coulomb barrier. Therefore, the influence of the short-range nuclear potential must be very weak. Thus, a TI pattern should be observable in the neighborhood of 0.40 MeV. Unfortunately, no experiment has been performed in this energy region.

However, there are measurements of ^{4}He + ^{4}He scattering at higher energies, and the experimental cross sections at 1.0 and 1.5 MeV exhibit TI patterns. These findings were theoretically justified in Ref. [2], where it was shown that the nuclear potential gives rise to new TI patterns at energies above the Coulomb barrier. Although the new TI energies cannot be calculated analytically, they can be easily determined by numerical procedures. First, one evaluates the function

$$\mathcal{D}(E) = \left[\frac{d^2\sigma(\theta)}{d\theta^2}\right]_{\theta=\pi/2}. \quad (29)$$

The TI energies are then given by the solutions of the equation $\mathcal{D}(E) = 0$.

Although the predictions of Mott scattering cannot be extended to systems where $E_{\rm C} \geqslant V_{\rm B}$, they can be used to help select systems where TI could be observed.

Table I shows the TI energies predicted in Mott scattering of a few identical light nuclei in comparison with their Coulomb barriers. The barriers were calculated by using the Akyüz–Winther potential [6,7]. Clearly, the ideal system for TI studies is ^{4}He + ^{4}He, where the $E_{\rm C}$ value lies well below the Coulomb barrier. Furthermore, there is the additional advantage that ^{4}He + ^{4}He scattering at near-barrier energies can be theoretically described with a real potential. This is because the lowest excited state of ^{4}He lies above ~20 MeV. Therefore all nonelastic channels are closed. Collisions of heavier identical nuclei are more complicated. Those collisions suffer a stronger influence of nuclear forces, so that the predictions of Mott scattering may not be so useful. It is then essential to include a nuclear potential in all calculations. This potential should be complex, to account for the influence of open inelastic and/or transfer channels.

1. ^{6}Li + ^{6}Li scattering

According to Eq. (28), the TI energy predicted in Mott scattering increases with the atomic number and decreases

TABLE II. Woods–Saxon parameters of the AW and of the phenomenological potentials for the ^{6}Li + ^{6}Li scattering case. All potential strengths are given in MeV and lengths given in fm. See text for details.

Pot.	U_0	W_0	r_{0r}	r_{0i}	a_r	a_i	r_{0C}
AW	−26.9	−21.0	1.15	1.15	0.54	0.54	1.06
WS-1	−5.0	−5.0	1.60	1.60	0.12	0.46	1.60
WS-2	−11.7	−6.9	1.40	1.50	0.46	0.73	1.30

with the spin of the nucleus. Then the next systems where the nuclear effects must be weak are ^{6}Li and ^{10}B (we note that there are no stable even-A Be isotopes). In this section we will investigate TI in ^{6}Li + ^{6}Li collisions. Since the TI energy in Mott scattering is below the Coulomb barrier (see Table I), it should not be significantly affected by the nuclear potential.

We consider three nuclear potentials: The first is the Akyüz–Winther (AW) potential [6], $U_{AW}(r)$. This potential is calculated by a double folding integral involving the projectile's and target's densities and a nucleon-nucleon interaction [8,9]. This integral is calculated within some approximations and the resulting potential is fit by a Woods–Saxon (WS) function. This procedure was applied to several systems and the parameters of the WS: V_0, r_0, and a, which were approximated by analytical functions of the mass numbers of the collision partners. We assume that the potential has an imaginary part with the same shape. This procedure was successfully used in the description of elastic and reaction cross sections for several systems [10]. In this way, we set

$$V_{AW}(r) = [U_0(r) + iW_0(r)]f_{WS}(r), \tag{30}$$

with

$$f_{WS}(r) = \frac{1}{1 + \exp[(r - R_0)/a]}. \tag{31}$$

The other two potentials considered in this section are phenomenological WS potentials with different sets of parameters. In these cases, different parameters are used for the real and for the imaginary parts of the WS. The first set of parameters, set 1, was taken from Ref. [11] whereas the second, set 2, was taken from Ref. [12].

The Coulomb potential is given by the usual approximation in heavy-ion scattering:

$$V_C(r) = \frac{Z^2e^2}{r} \quad \text{for } r \geqslant R_C$$
$$= \frac{Z^2e^2}{2R_C}\left(3 - \frac{r^2}{R_C^2}\right) \quad \text{for } r < R_C.$$

Above, $R_C = 2r_{0C}A^{1/3}$ is the Coulomb radius and Z and A are the atomic and the mass numbers, respectively, of the identical collision partners.

The parameters of the nuclear potentials and the Coulomb potential used in our ^{6}Li + ^{6}Li scattering calculations are listed in Table II.

The second derivatives of the elastic cross section in ^{6}Li + ^{6}Li scattering at 90 degrees ($\theta = \pi/2$) for the three potentials are shown in Fig. 1 as functions of the collision energy. We note

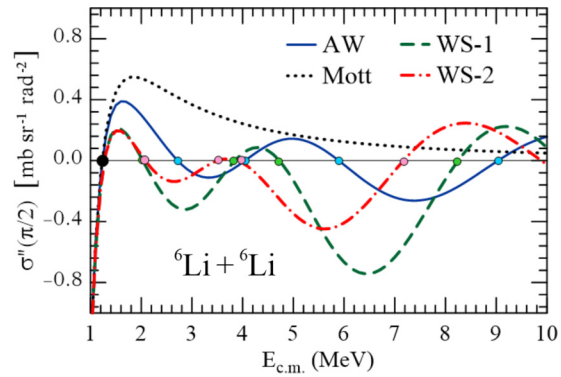

FIG. 1. Second derivatives of the differential cross sections for ^{6}Li + ^{6}Li elastic scattering, at $\theta = \pi/2$. The results for the three potentials considered in the text are shown as functions of collision energy. The solid circles indicate the TI energies.

that there are several energies where the second derivatives vanish. However, only at the lowest energy the predictions of the three potentials coincide. The next-higher TI energy is the same for the two phenomenological WS potentials, but not for the AW potential. Note that the remaining TI energies are strongly dependent on the nuclear potential employed.

Figure 2 shows angular distributions in the vicinity of 90 degrees calculated with the three potentials. The results are for the collision energies $E = 1.25$ [Fig. 2(a)] and $E = 2.05$ MeV [Fig. 2(b)]. The three angular distributions at $E = 1.25$ MeV are very flat. This is consistent with Fig. 1, which indicates that the three potentials have a TI energy very close to 1.25 MeV. The TI energies for the AW potential and for the WS potentials with parameter sets 1 and 2 are respectively 1.24, 1.28, and 1.28 MeV. Note that these TI energies are also close to that in

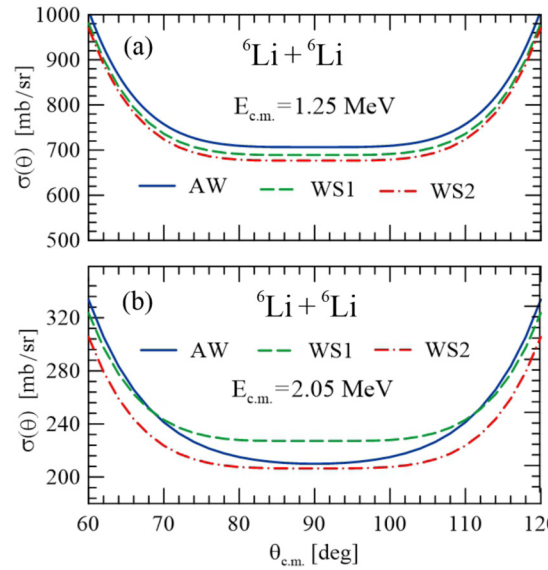

FIG. 2. Angular distributions of ^{6}Li + ^{6}Li scattering at 1.25 and 2.05 MeV calculated with the AW potential (blue solid lines) and with the phenomenological WS potentials with set 1 (green dashed lines) and set 2 (red dot-dashed lines).

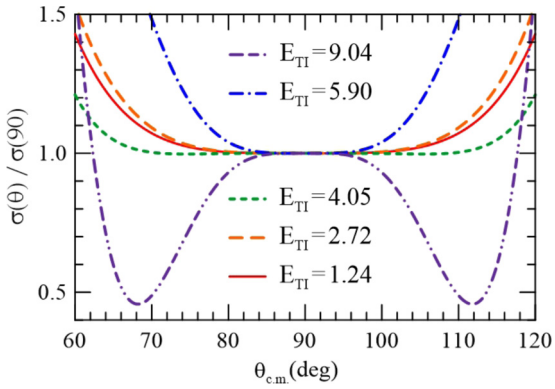

FIG. 3. Angular distributions of ^{6}Li + ^{6}Li scattering at the TI energies below 10 MeV. The curves correspond to calculations with the Akyüz–Winther potential, normalized with respect to their values at $\theta = 90$ degrees.

Mott scattering (see Table I). On the other hand, the angular distributions at 2.05 MeV show different patterns (see Fig. 3). The curves for the two phenomenological WS potentials are very flat, whereas that for the AW potential exhibits a minimum at 90 degrees. Again, this is consistent with Fig. 1: the second derivatives for the two phenomenological potentials vanish at 90 degrees, while the one for the AW potential is positive.

Now we investigate the influence of the collision energy in the TI pattern. For this purpose, we show the angular distributions at all TI energies below 10 MeV. For simplicity, we limit this study to the AW potential. We note that, for most energies, the flat angular region is $\theta \approx 90 \pm 10$ degrees, but at 4.05 MeV it is $\theta \approx 90 \pm 20$ degrees. We emphasize again that these results are strongly dependent on the nuclear potential employed, which suggests the experimental determination of the TI energies and the angular distributions at those energies are useful constraints on the nuclear optical potential.

2. $^{10}B + ^{10}B$ scattering

Now we investigate TI in ^{10}B + ^{10}B scattering. In this case the TI energy predicted in Mott scattering exceeds the Coulomb barrier by about 60%. Thus, the choice of the nuclear potential is expected to play an even more crucial role than in the case of ^{6}Li + ^{6}Li. As in the previous section, we perform calculations with the AW and with two phenomenological potentials. The latter are the WS potential with two sets of parameters, which we label by A and B, taken from Ref. [13]. The WS parameters of the AW and of the phenomenological potential are listed in Table III, together with the radius parameter of the Coulomb potential.

Figure 4 shows the second derivatives of the angular distributions, $\mathcal{D}(E)$, as defined in Eq. (29) for the AW and the two phenomenological WS potentials, as well as for the Mott-scattering case. In each case, the TI energies are indicated by solid circles. The conclusions of this analysis are summarized in Table IV. We notice that the results are strongly dependent on the nuclear potential for all of the energies considered. Here, the TI energies for the three potentials are systematically different. Similar situations are expected to occur in collisions of other heavier systems. Thus TI could to be a useful tool to investigate the nuclear interaction in collisions of identical nuclei.

TABLE III. The parameters of the AW and of the phenomenological potentials of Ref. [13] for ^{10}B + ^{10}B scattering. Potential strengths are given in MeV and lengths are given in fm. See text for details.

Pot.	U_0	W_0	r_{0r}	r_{0i}	a_r	a_i	r_{0C}
AW	−34.1	−26.6	1.16	1.16	0.57	0.57	1.06
WS-A	−70.0	−10.0	1.05	1.05	0.50	0.50	1.06
WS-B	−500.0	−19.5	1.05	1.05	0.40	0.40	1.06

Figure 5 shows angular distributions calculated by using the three potentials discussed in the text, at three of the collision energies listed in Table IV. This means that each one is a TI energy for one of these potentials. At 4.8 MeV, the angular distribution for the WS potential with set B (red dot-dashed line) is very flat, whereas those for the other two potentials exhibit maxima at 90 degrees. This is consistent with the indication of Table IV. At 7.8 MeV, the angular distribution of the AW potential is flat, whereas the other two have minima at 90 degrees. This is also consistent with the analysis of the second derivative, presented in Table IV. Finally, at 9.0 MeV, the angular distribution for the WS potential with set A is flat, whereas the one for the AW potential has a maximum at 90 degrees and the one for the WS with set B has a minimum. Again, this is consistent with the indications of Table IV.

IV. THE FUSION CROSS SECTION

The fusion cross section for an unpolarized collision is given by

$$\sigma_F = \frac{1}{(2s+1)^2}\frac{1}{|A|^2}\frac{k}{E}\sum_{\mu_1\mu_2}\langle\Psi^{(+)}_{\mu_1\mu_2}| - W|\Psi^{(+)}_{\mu_1\mu_2}\rangle. \quad (32)$$

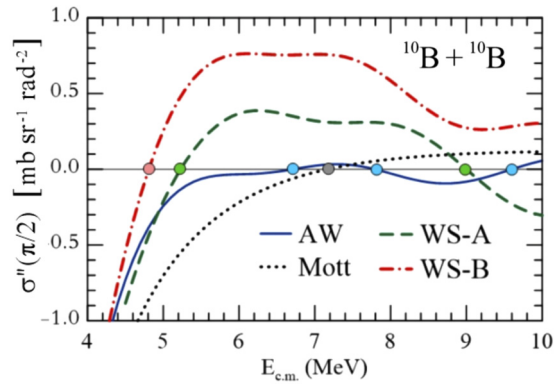

FIG. 4. Second derivatives of the angular distribution of ^{10}B + ^{10}B scattering with respect to θ, taken at $\theta = \pi/2$. The curves correspond to results for the three nuclear potentials discussed in the text, and for the Mott-scattering case. The solid circles indicate the TI energies.

TABLE IV. Behavior of the angular distributions for the three potentials of Table III at the TI energies of each individual potential. The ↑ symbol indicates that the angular distribution at $\pi/2$ has a maximum, ↓ that it has a minimum, and "TI" indicates "transverse isotropy."

$E_{\rm TI}$ (MeV)	AW	WS-A	WS-B
4.8	↑	↑	TI
5.2	↑	TI	↓
6.7	TI	↓	↓
7.8	TI	↓	↓
9.0	↑	TI	↓
9.6	TI	↑	↓

Inserting the explicit form of the wave function [Eq. (8)] in the above equation and using the fact that the imaginary potential is diagonal in the $|S\nu\rangle$ basis, one gets

$$\sigma_{\rm F} = -\frac{1}{(2s+1)^2}\frac{k}{2|A|^2E}\sum_{S=0}^{2s}\sum_{\nu=-S}^{S}\sum_{\mu_1\mu_2}|\langle S\nu|s\mu_1 s\mu_2\rangle|^2 \times[\langle\psi|W|\psi\rangle + (-)^S\{\langle\psi|W\mathbb{P}|\psi\rangle + \langle\psi|\mathbb{P}^\dagger W|\psi\rangle\} + (-)^{2S}\langle\psi|\mathbb{P}^\dagger W\mathbb{P}|\psi\rangle].$$

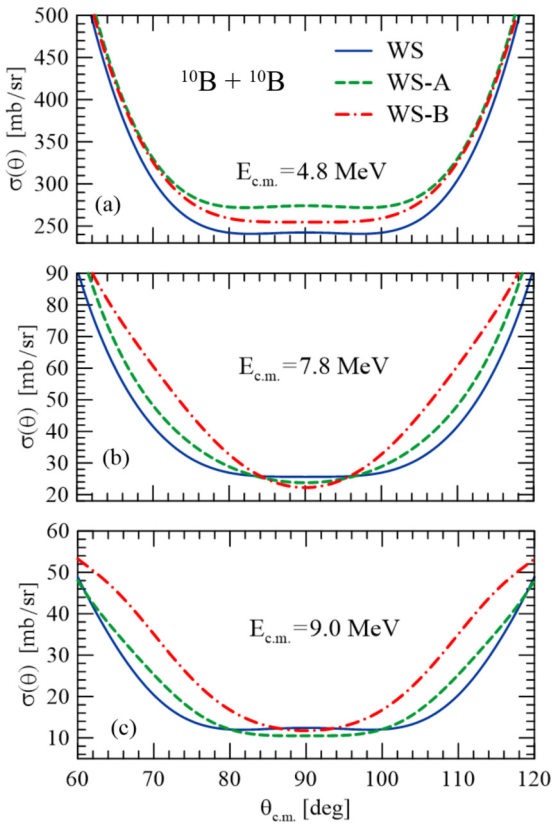

FIG. 5. Angular distributions in ^{10}B + ^{10}B at three energies, calculated for the three potentials of Table III. For details see text.

Carrying out the summation over μ_1, μ_2, and ν, one gets

$$\sigma_{\rm F} = -\frac{1}{(2s+1)^2}\frac{k}{2|A|^2E}\sum_{S=0}^{2s}(2S+1) \times[\langle\psi|W|\psi\rangle + (-)^S\{\langle\psi|W\mathbb{P}|\psi\rangle + \langle\psi|\mathbb{P}^\dagger W|\psi\rangle\} + (-)^{2S}\langle\psi|\mathbb{P}^\dagger W\mathbb{P}|\psi\rangle]. \quad (33)$$

Above, we have used the symmetry property of the Clebsch–Gordan coefficients,

$$\sum_{\mu_1\mu_2}|\langle S\nu|s\mu_1 s\mu_2\rangle|^2 = 1. \quad (34)$$

Next, we use the relations

$$\mathbb{P}^\dagger = \mathbb{P}, \quad \mathbb{P}^2 = \mathbf{1}, \quad [\mathbb{P}, W] = 0, \quad (-)^{2S} = 1, \quad (35)$$

and get

$$\sigma_{\rm F} = -\frac{1}{(2s+1)^2}\frac{1}{|A|^2}\frac{k}{E}\sum_{S=0}^{2s}(2S+1) \times[\langle\psi|W|\psi\rangle + (-)^S\langle\psi|W\mathbb{P}|\psi\rangle]. \quad (36)$$

A. The partial-wave projection

Next, we carry out the angular-momentum expansion of the wave function in coordinate space [see Eq. (3.125a) of Ref. [9]] for an incident wave along the z axis ($\hat{k}_0 = \hat{z}$),

$$\psi(\mathbf{r}) = A\sum_l\sqrt{4\pi(2l+1)}Y_{l0}(\hat{\mathbf{r}})e^{i\sigma_l}i^l\frac{u_l(kr)}{kr}, \quad (37)$$

where we have used the relation $Y_{lm}(\hat{\mathbf{z}}) = \sqrt{(2l+1)/4\pi}\delta_{m,0}$. The partial-wave expansion of $\mathbb{P}(\psi\mathbf{r})$ can be trivially obtained from the above equation by using the property $Y_{l0}(-\hat{\mathbf{r}}) = (-)^l Y_{l0}(\hat{\mathbf{r}})$. One gets

$$\mathbb{P}\psi(\mathbf{r}) = A\sum_l(-)^l\sqrt{4\pi(2l+1)}Y_{l0}(\hat{\mathbf{r}})e^{i\sigma_l}i^l\frac{u_l(kr)}{kr}. \quad (38)$$

Note that we are assuming that the radial wave function is not dependent on the total angular momentum $\mathbf{J} = \mathbf{L} + \mathbf{S}$. This condition is clearly satisfied if there is no spin-orbit term in the projectile-target interaction.

By using these expansions in Eq. (36) and considering that W is a central potential, we get

$$\sigma_{\rm F} = -\frac{4\pi}{(2s+1)^2}\frac{k}{E}\sum_{S=0}^{2s}(2S+1)\sum_{l,l'}\sqrt{(2l+1)(2l'+1)} \times e^{i(\sigma_{l'}-\sigma_l)}i^{l'-l}[1+(-)^{S+l'}]\int Y^*_{l0}(\hat{\mathbf{r}})Y_{l'0}(\hat{\mathbf{r}})d\Omega \times\int\frac{u^*_l(kr)}{k}W(r)\frac{u_{l'}(kr)}{k}dr, \quad (39)$$

and, by using the orthonormality of the spherical harmonics,

one gets

$$\sigma_{\rm F} = -\frac{1}{(2s+1)^2}\frac{4\pi}{kE}\sum_{S=0}^{2s}(2S+1)\sum_l(2l+1) \times[1+(-)^{S+l}]\int|u_l(kr)|^2W(r)dr, \quad (40)$$

or

$$\sigma_{\rm F} = \frac{1}{(2s+1)^2}\frac{\pi}{k^2}\sum_{S=0}^{2s}(2S+1)\sum(2l+1)[1+(-1)^{l+S}]T_l, \quad (41)$$

with

$$T_l = \frac{4k}{E}\int_0^\infty[-W(r)]|u_l(kr)|^2dr. \quad (42)$$

Equation (41) can be simplified if one rewrites it in the form

$$\sigma_{\rm F} = \frac{\pi}{k^2}\sum_l(2l+1)T_l\left[\frac{N_-+N_-}{(2s+1)^2}\right] + \frac{\pi}{k^2}\sum_l(2l+1)(-)^lT_l\left[\frac{N_+-N_-}{(2s+1)^2}\right], \quad (43)$$

and then use Eq. (22). The resulting cross section can be put in the form

$$\sigma_{\rm F} = \sigma_0 + \sigma_{\rm osc}, \quad (44)$$

where

$$\sigma_0 = \frac{\pi}{k^2}\sum_l(2l+1)T_l \quad (45)$$

is the fusion cross section for distinguishable collision partners, and

$$\sigma_{\rm osc} = \left[\frac{(-)^{2s}}{2s+1}\right]\frac{\pi}{k^2}\sum_l(-1)^l(2l+1)T_l \quad (46)$$

is a correction arising from the exchange symmetry. As we show in the next section, this term oscillates with the collision energy.

B. Analytical insight of energy oscillations in fusion cross section

There are two types of energy oscillations in the fusion cross section:

(1) Oscillations related to the discrete nature of the l sum:

$$\sigma_0 = \frac{\pi}{k^2}\sum_l(2l+1)T_l. \quad (47)$$

This is present in all fusion cross sections; however, they are quite small and are very difficult to observe due to energy-resolution limitations.

(2) Oscillations arising from the symmetry requirement in the case of fusion of identical nuclei, exemplified by Eq. (46). This type of energy oscillations is a natural consequence of the odd-even staggering contained in the l sum.

To exhibit clearly these two types of oscillations we resort to an alternative representation of the l sum; namely, the Poisson formula. In this representation, the sum

$$\mathcal{S}(E) \equiv \sum_l(2l+1)T_l(E) \quad (48)$$

is given by the series of integrals over the continuous variable $\lambda = l + 1/2$,

$$\mathcal{S}(E) = 2\sum_{m=0,\pm1,\ldots}(-)^m\int\lambda T(\lambda,E)e^{2i\pi m\lambda}d\lambda, \quad (49)$$

or

$$\mathcal{S}(E) = \mathcal{S}_0(E) + \mathcal{S}_{-1}(E) + \mathcal{S}_{+1}(E) + \cdots, \quad (50)$$

with

$$\mathcal{S}_m(E) = 2(-)^m\int\lambda T(\lambda,E)e^{2i\pi m\lambda}d\lambda. \quad (51)$$

Inspecting the above equation, one concludes that $\mathcal{S}_0(E)$ is real and the remaining terms are complex, satisfying the relation

$$\mathcal{S}_m(E) = \mathcal{S}^*_{-m}(E). \quad (52)$$

For $m \neq 0$, the integrand of Eq. (51) oscillates, and the period of oscillations decreases as $|m|$ increases. This produces cancellations, so that Eq. (50) is dominated by the term with $m = 0$. Truncating the series of Eq. (49) after $|m| = 1$ and using the result in Eqs. (48) and (47), the fusion cross section takes the form

$$\sigma_0(E) = \sigma_0^{(0)}(E) + \Delta\sigma_0(E), \quad (53)$$

where

$$\sigma_0^{(0)}(E) = \frac{\pi}{k^2}\mathcal{S}_0(E) \quad (54)$$

is the leading term and

$$\Delta\sigma_0(E) = \frac{\pi}{k^2}[\mathcal{S}_{-1}(E)+\mathcal{S}_{+1}(E)] = \frac{2\pi}{k^2}{\rm Re}\{\mathcal{S}_{-1}(E)\} \quad (55)$$

is a small correction, which oscillates with the collision energy.

It is convenient to introduce the integral

$$I_n(E) = \int_0^\infty d\lambda\lambda T(\lambda,E)e^{i\pi n\lambda} \quad (56)$$

so that we can write

$$\mathcal{S}_m(E) = 2(-)^m I_{2m}(E) \quad (57)$$

and

$$\Delta\sigma_0(E) = -\frac{4\pi}{k^2}{\rm Re}\{I_2(E)\}. \quad (58)$$

In the case of identical nuclei, the cross section gets an additional term $\sigma_{\rm osc}$ [see Eqs. (44)], which is given by the parity-dependent partial-wave sum of Eq. (46). Using the Poisson representation of this sum and writing

$$(-)^l = e^{i\pi l} = e^{i\pi(\lambda-1/2)} = -ie^{i\pi\lambda},$$

the cross section $\sigma_{\rm osc}$ takes the form

$$\sigma_{\rm osc} = \frac{(-)^{2s}}{2s+1}\frac{\pi}{k^2}\sum_{m=0,\pm1,\ldots} \mathcal{Z}_m(E), \tag{59}$$

with

$$\mathcal{Z}_m(E) = -2i(-)^m \int d\lambda \lambda T(\lambda, E) e^{i\pi(2m+1)\lambda}, \tag{60}$$

or

$$\mathcal{Z}_m(E) = -2i(-)^m I_{2m+1}(E). \tag{61}$$

The terms $\mathcal{Z}_m(E)$ and the integrands in the above equation are oscillating functions of λ. Then the leading terms, which oscillate more slowly, are those for $m = 0$ and $m = -1$. These terms are related by the expression

$$\mathcal{Z}_{-1}(E) = \mathcal{Z}_0^*(E). \tag{62}$$

Then, neglecting the contributions from the remaining terms, the cross section of Eq. (59) becomes

$$\begin{aligned}\sigma_{\rm osc}(E) &= \frac{(-)^{2s}}{2s+1}\frac{\pi}{k^2}[\mathcal{Z}_0(E) + \mathcal{Z}_{-1}(E)] \\ &= \frac{(-)^{2s}}{2s+1}\frac{2\pi}{k^2}{\rm Re}\{\mathcal{Z}_0(E)\},\end{aligned} \tag{63}$$

or

$$\sigma_{\rm osc}(E) = \frac{(-)^{2s}}{2s+1}\frac{4\pi}{k^2}{\rm Im}\{I_1(E)\}. \tag{64}$$

The relative importance of the oscillatory terms in Eqs. (58) and (64) can be better assessed if an analytical form for the transmission coefficient $T(\lambda, E)$ is employed. This is supplied by the Hill–Wheeler formula [14,15], based on the parabolic approximation of the λ-dependent effective interaction. The potential is approximated by the parabola

$$V(r) = B_\lambda - \tfrac{1}{2}\mu\omega_\lambda^2(r - R_\lambda)^2,$$

where B_λ, R_λ, and $\hbar\omega_\lambda$ are respectively the height, the radius, and the curvature parameter of the parabolic approximation to the barrier of the effective potential for angular momentum λ. The transmission coefficient through this parabolic barrier can be evaluated exactly, and the result is [14]

$$T(\lambda, E) = \frac{1}{1 + \exp\left[2\pi(B_\lambda - E)/\hbar\omega_\lambda\right]}. \tag{65}$$

Wong neglected the angular-momentum dependence of the radius and the curvature parameter. He approximated

$$R_\lambda \simeq R_{\lambda=0} \equiv R_{\rm B}$$

and

$$\hbar\omega_\lambda \simeq \hbar\omega_{\lambda=0} \equiv \hbar\omega.$$

In this way, the barrier height for angular momentum λ is given by

$$B_\lambda = V_{\rm B} + \frac{\hbar^2\lambda^2}{2\mu R_{\rm B}^2},$$

where we have introduced the notation: $V_{\rm B} \equiv B_{\lambda=0}$. With this approximation, the term $m = 0$ of the Poisson series can be evaluated analytically. The result, known in the literature as the Wong formula [15], is

$$\sigma^{\rm W}(E) = \frac{\hbar\omega R_{\rm B}^2}{2E}\ln\left[1 + \exp\left(\frac{2\pi}{\hbar\omega}(E - V_{\rm B})\right)\right]. \tag{66}$$

The Wong formula works for heavy systems but is very inaccurate for light heavy ions, below and above the Coulomb barrier. Rowley and Hagino [16] showed that it can be significantly improved if one replaces $R_{\rm B}$ and $\hbar\omega$ by the parameters associated with the grazing angular momentum, denoted respectively by $R_{\rm E}$ and $\hbar\omega_{\rm E}$, and replace also

$$V_{\rm B} \to V_{\rm E} = V_{\rm N}(R_{\rm E}) + V_{\rm C}(R_{\rm E}).$$

The term of order zero of the Poisson formula then becomes

$$\sigma_0^{(0)}(E) = \frac{\hbar\omega_{\rm E} R_{\rm E}^2}{2E}\ln\left[1 + \exp\left(\frac{2\pi}{\hbar\omega_{\rm E}}(E - V_{\rm E})\right)\right]. \tag{67}$$

The calculation of the other terms of the Poisson series is more complicated. To evaluate $\Delta\sigma_0(E)$ and $\sigma_{\rm osc}$, one first rewrites the transmission coefficient in terms of the angular momentum λ and its grazing value λ_g given by the relation

$$\lambda_g = \left[\frac{2\mu R_{\rm E}^2}{\hbar^2}(E - V_{\rm E})\right]^{1/2}. \tag{68}$$

One gets

$$T(\lambda, E) = \left\{1 + \exp\left[\frac{2\pi}{\hbar\omega_{\rm E}}\left(\frac{\hbar^2}{2\mu R_{\rm E}^2}\left(\lambda^2 - \lambda_g^2\right)\right)\right]\right\}^{-1}. \tag{69}$$

This expression is then used in Eq. (56). The resulting integrals cannot be calculated analytically. However, approximate expressions can be obtained [16] by evaluating the integrals in the complex plane. For energies sufficiently above the barrier [$(E - V_{\rm E}) \gg \hbar\omega_{\rm E}/2$], one gets for $n \neq 0$ (see Appendix B for details)

$$I_n(E) = i\frac{\mu\hbar\omega_{\rm E} R_{\rm E}^2}{\hbar^2} e^{-n\xi} e^{in\pi\lambda_g}, \tag{70}$$

with

$$\xi = \frac{\mu\hbar\omega_{\rm E} R_{\rm E}^2}{2\hbar^2\lambda_g}. \tag{71}$$

Then, inserting the above result into Eq. (58), replacing $\lambda_g \to l_g + 1/2$, and expressing k^2 in terms of E, one obtains

$$\Delta\sigma_0(E) = -2\pi\frac{\hbar\omega_{\rm E}}{E} R_{\rm E}^2 e^{-2\xi}\sin(2\pi l_g). \tag{72}$$

Repeating the same procedure in Eq. (64), one gets

$$\sigma_{\rm osc}(E) = \frac{(-)^{2s}}{2s+1} 2\pi\frac{\hbar\omega_{\rm E}}{E} R_{\rm E}^2 e^{-\xi}\sin(\pi l_g). \tag{73}$$

As a result of the damping factors, the symmetry-related energy oscillation is larger in magnitude than the discrete-l-related energy oscillation. The periods of the oscillation of

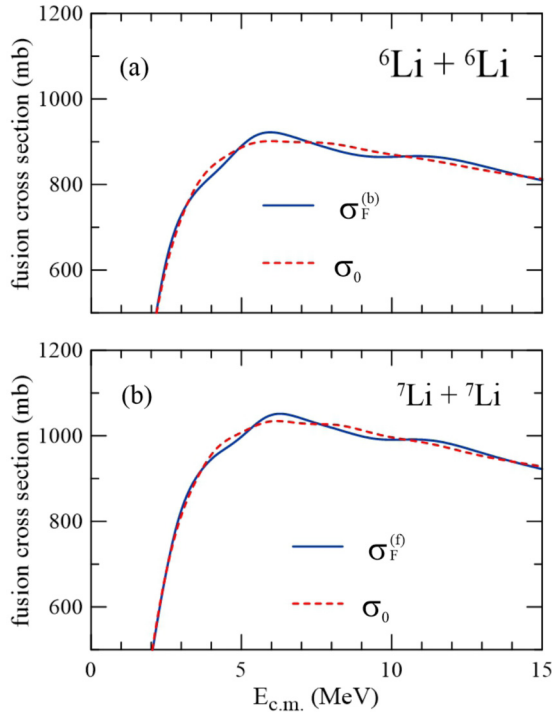

FIG. 6. Fusion cross sections for the identical projectile-target systems (a) ^{6}Li + ^{6}Li and (b) ^{7}Li + ^{7}Li. For details see the text.

$\Delta\sigma_0(E)$ (P) and $\sigma_{osc}(E)$ (P') are

$$P(E) = \frac{dE}{d\lambda_g} = \frac{\hbar^2\lambda_g}{\mu R_E^2}, \tag{74}$$

$$P'(E) = 2\frac{dE}{d\lambda_g} = 2\frac{\hbar^2\lambda_g}{\mu R_E^2}. \tag{75}$$

Thus the fusion cross section for identical nuclei exhibits symmetry-related energy oscillations superimposed on twice-as-rapid smaller-amplitude discrete-l-related oscillations. It is very difficult to discern the rapid oscillations because they are very tiny. However, the symmetry-related oscillation have been observed for $s = 0$ [16,17]. In the application to follow we numerically evaluate the fusion cross section for the systems ^{6}Li + ^{6}Li ($s = 1$) and ^{7}Li + ^{7}Li ($s = 3/2$), guided by the results of this section.

C. Applications

1. Fusion in ^{6}Li + ^{6}Li and ^{7}Li + ^{7}Li collisions

In this section we study fusion of the ^{6}Li + ^{6}Li and ^{7}Li + ^{7}Li systems. The ^{6}Li nucleus is treated as a boson with spin $s = 1$ and ^{7}Li is treated as a fermion with spin $s = 3/2$. We adopt the Akyüz–Winther potential [6] for the real part of the nucleus-nucleus interaction, and a short-range strong absorption potential for its imaginary part. More precisely, we employ a Woods–Saxon function with parameters $W_0 = -50$ MeV, $r_{0i} = 1.0$ fm, and $a_i = 0.2$ fm.

Fusion cross sections for the ^{6}Li + ^{6}Li and ^{7}Li + ^{7}Li systems are shown respectively in Figs. 6(a) and 6(b). The blue solid lines are cross sections including exchange effects.

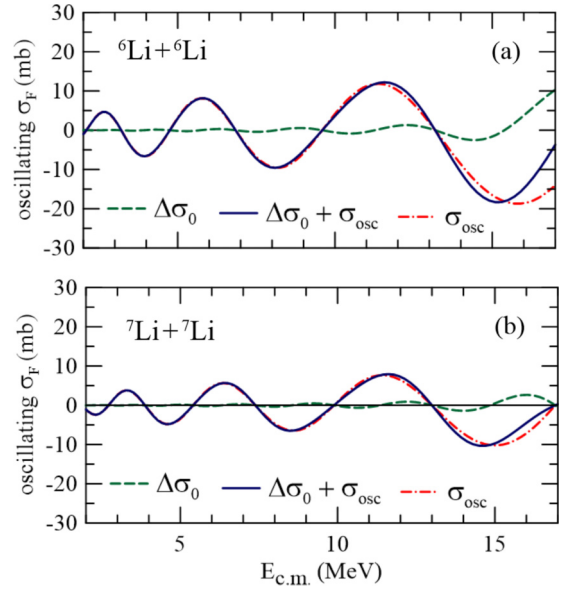

FIG. 7. The oscillatory terms, $\Delta\sigma_0(E)$ and $\sigma_{osc}(E)$ of Eqs. (72 and 73) vs the center-of-mass energy for the systems ^{6}Li + ^{6}Li and ^{7}Li + ^{7}Li. See text for details.

These cross sections are denoted by $\sigma_F^{(b)}$ in case of bosons (^{6}Li), and by $\sigma_F^{(f)}$ in the case of fermions (^{7}Li). The red dashed lines correspond to the cross sections σ_0, where exchange effects are neglected. It is clear that the effects of exchange are very small. The amplitudes of the oscillations for the two systems are quite close, although in the case of ^{7}Li + ^{7}Li the oscillations seem to be slightly weaker. Weaker oscillations in the case of ^{7}Li would be expected for two reasons. The first is that the oscillation amplitude decreases with the mass [16]. The second is that it also decreases with the spin of the collision partners, as Eq. (46) indicates.

Figure 7 shows results of the analytical approximation for the oscillatory terms in the fusion cross sections of ^{6}Li + ^{6}Li [Fig. 7(a)] and ^{7}Li + ^{7}Li [Fig. 7(b)]. The details of the calculations are presented in Appendix B. The figure shows $\Delta\sigma_0$ (green dashed lines), σ_{osc} (red dot-dashed lines), and the sum of the two (blue solid lines), which corresponds to the total correction to the improved Wong formula of Eq. (72). The results are shown from an energy just above the Coulomb barrier to 15 MeV. This upper limit is slightly below the critical energy for the ^{6}Li-^{6}Li collision ($E_{crit} = 17.6$ MeV), above which the grazing angular momenta used in the calculations are not defined. Clearly, the oscillations arising from the discrete nature of l ($\Delta\sigma_0$) are much weaker than those associated with exchange (σ_{osc}), except at the highest energies.

Comparing σ_{osc} for the ^{6}Li + ^{6}Li and ^{7}Li + ^{7}Li systems (red dot-dashed lines in the two panels), one observes two interesting points: The first is that the oscillations for the two systems are approximately in phase. At first sight, this is an unexpected result. The cross section σ_{osc} is proportional to exchange factor, $(-)^{2s}/(2s+1)$, which is positive for ^{6}Li and negative for ^{7}Li. From this point of view one would expect oscillations with opposite phases. However, the exchange factor is not the only difference in the two cross sections. Since

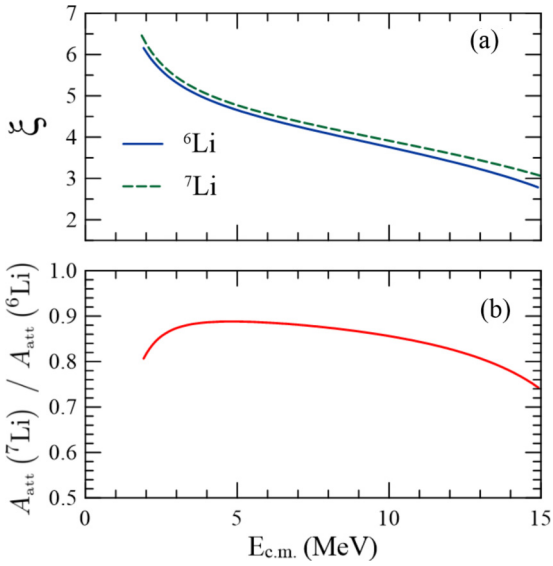

FIG. 8. Damping of $\sigma_{osc}(E)$ in the $^6\text{Li}+^6\text{Li}$ and $^7\text{Li}+^7\text{Li}$ collisions: panel (a) shows the damping parameter, ξ, in the two cases; panel (b) shows the ratio of the two attenuation factors ($A_{tt} = \exp(-\pi\xi)$) for the two Li systems. See text for details.

the potential barriers for the two systems are different, the λ-dependent transmission coefficients used in the calculations are not the same. Then, the combined effect of these two factors cannot be guessed. To check this point, we performed a new calculations for the $^6\text{Li}+^6\text{Li}$ system adopting the artificial spin value $s = 3/2$. In this case, the only difference between the cross sections for the two spin values is the exchange factor. Then, as expected, the oscillations in the two cross sections have opposite phases.

The second feature is that the amplitude of the oscillations for ^{7}Li (measured at $E \sim 11$ MeV) is about 65% of the one for ^{6}Li. To justify this result, we recall that σ_{osc} is proportional to two factors [see Eq. (73)]. The first is the exchange factor, with modulus $1/(2s+1)$. That is, it is equal to $1/4$ for ^{7}Li and

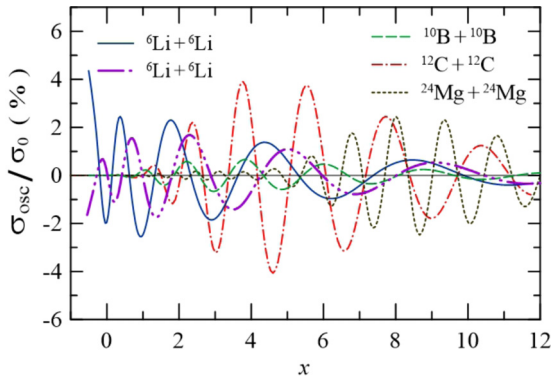

FIG. 9. Influence of the spin and the mass of the identical nuclei on the exchange effects. The figure shows the ratio σ_{osc}/σ_0 for several systems as functions of the dimensionless energy variable, $x = (E - V_B)/\hbar\omega$. Clearly, the importance of exchange effects (measured by the amplitude of the oscillations) decreases with the mass and the spin.

TABLE V. Barrier parameters for different systems. V_B and $\hbar\omega$ are given in MeV and R_B is given in fm.

System	V_B (MeV)	R_B (fm)	$\hbar\omega$ (MeV)
$^6\text{Li}+^6\text{Li}$	1.7	7.0	2.4
$^7\text{Li}+^7\text{Li}$	1.6	7.4	2.1
$^{10}\text{B}+^{10}\text{B}$	4.4	7.6	2.8
$^{12}\text{C}+^{12}\text{C}$	6.1	7.8	2.9
$^{24}\text{Mg}+^{24}\text{Mg}$	21.8	8.8	3.4

$1/3$ for ^{6}Li. The second is the energy-dependent attenuation factor

$$A_{att} = \exp(-\xi),$$

which is different for the two Li isotopes. The effects of the damping is illustrated in Fig. 8. Figure 8(a) shows the damping parameter ξ for the two Li systems as functions of the collision energy. One observes that the curves for the two systems are close, and that the one for ^{7}Li is slightly higher. Therefore, the attenuation factors for ^{7}Li must be smaller than those for ^{6}Li. This behavior is confirmed in the curve in Fig. 8(b), which shows the ratio of the two attenuation factors. Indeed, the ratio $A_{att}(^6\text{Li})/A_{att}(^7\text{Li})$, corresponding to the red solid line, is less than unity in the whole energy range.

2. *Comparison with heavier systems*

The mass dependence of the oscillations are investigated in Fig. 9, where we compare the oscillating cross section in collisions of several identical nuclei. We consider ^{6}Li (spin 1), ^{7}Li (spin 3/2), ^{10}B (spin 3), ^{12}C (spin 0), and ^{24}Mg (spin 0). In this case, we plot the ratio σ_{osc}/σ_0, instead of σ_{osc}, against the reduced energy $x = (E - V_B)/\hbar\omega$. The use of reduced energies is a common procedure in comparisons of cross sections for different systems [18–20]. For any system, the barrier energy corresponds to $x = 0$. The barrier parameters for these systems are given in Table V.

First, one notices that the amplitude of the oscillations for $^6\text{Li}+^6\text{Li}$ increases at very low energies, which was not observed in the previous figures. The reason is that σ_0 decreases rapidly in this reaction, leading to a pronounced increase of the ratio σ_{osc}/σ_0. Comparing the curves for the other systems, one finds that the strongest oscillations occur in the case of $^{12}\text{C}+^{12}\text{C}$, although its mass is twice that of the $^6\text{Li}+^6\text{Li}$ system. This behavior can be traced back to the spin zero of ^{12}C. Thus, the spin dependence is much stronger that the mass dependence.

V. CONCLUSIONS

In this paper we have reported a general discussion of the elastic scattering and fusion of identical nuclei with arbitrary spin. The fusion cross section exhibits two types of energy oscillations. The first, related to the discrete nature of the orbital angular momentum and taking place even in the more general case of fusion of nonidentical nuclei, is small and rather difficult to discern in the data. The second type of oscillations is exclusive to identical systems and related to the spatial

symmetry (antisymmetry) of the system. The corresponding oscillating term in the cross section is damped by the spin factor $(-)^{2s}/(2s+1)$. Accordingly, the higher the spin of the nuclei, the less important is the symmetry-related oscillating term. The same finding was obtained for the elastic-scattering cross section. Applications to light heavy-ion systems were made. The bosonic system $^6\mathrm{Li}+{}^6\mathrm{Li}$ and the fermionic system $^7\mathrm{Li}+{}^7\mathrm{Li}$ were carefully studied. The phenomenon of transverse isotropy (TI) the near flat angular distribution reached at a critical value of energy [1,2] in the angular distribution was revisited and discussed at a region of energy where the nuclear potential is significant. The same analysis was carried out for the slightly heavier system, $^{10}\mathrm{B}+{}^{10}\mathrm{B}$. We believe that a careful study of these types of oscillations both in the context of fusion and through the TI in the elastic scattering of identical nuclei could shed light on fundamental issues such as the disappearance of coherence, as well as supply useful information about the interacting system.

ACKNOWLEDGMENTS

The work was supported in part by the CNPq, CAPES, FAPERJ, FAPESP (Brazil), and by the PEDECIBA and ANII (Uruguay). M.S.H. acknowledges support from the CAPES/ITA Senior Visiting Professor Fellowship Program. A.J.T. acknowledges financial support from the French committee of the Brafitec program.

APPENDIX A: AN ALTERNATIVE EXPRESSION FOR σ_{F}

An alternative expression for the cross section can be obtained in terms of the wave functions with even (ψ_+) and odd (ψ_-) parities,

$$|\psi_+\rangle = \frac{|\psi\rangle + \mathbb{P}|\psi\rangle}{\sqrt{2}}, \tag{A1}$$

$$|\psi_-\rangle = \frac{|\psi\rangle - \mathbb{P}|\psi\rangle}{\sqrt{2}}. \tag{A2}$$

Writing the inverse transformations,

$$|\psi\rangle = \frac{|\psi_+\rangle + |\psi_-\rangle}{\sqrt{2}}, \tag{A3}$$

$$\mathbb{P}|\psi\rangle = \frac{|\psi_+\rangle - |\psi_-\rangle}{\sqrt{2}}, \tag{A4}$$

and inserting them into Eq. (34), we get

$$\begin{aligned}\sigma_{\mathrm{F}} = &-\frac{1}{(2s+1)^2}\frac{1}{2|A|^2}\frac{k}{E}\sum_{S=0}^{2s}(2S+1)\\ &\times[\langle\psi_+|W|\psi_+\rangle + \langle\psi_-|W|\psi_-\rangle\\ &+ (-1)^S(\langle\psi_+|W|\psi_+\rangle - \langle\psi_-|W|\psi_-\rangle)].\end{aligned} \tag{A5}$$

Re-ordering the terms of the above equation, it can be put in the form

$$\begin{aligned}\sigma_{\mathrm{F}} =&\frac{1}{2}\sigma_+\left[\frac{N_+ + N_-}{(2s+1)^2} + \frac{N_+ - N_-}{(2s+1)^2}\right]\\ &+\frac{1}{2}\sigma_-\left[\frac{N_+ + N_-}{(2s+1)^2} - \frac{N_+ - N_-}{(2s+1)^2}\right],\end{aligned} \tag{A6}$$

with

$$\sigma_\pm = -\frac{1}{|A|^2}\frac{k}{E}\langle\psi_\pm|W|\psi_\pm\rangle. \tag{A7}$$

Next, we use Eq. (22) in Eq. (A6) to get

$$\sigma_{\mathrm{F}} = \frac{1}{2}\sigma_+\left[1 + \frac{(-)^{2s}}{2s+1}\right] + \frac{1}{2}\sigma_-\left[1 - \frac{(-)^{2s}}{2s+1}\right]. \tag{A8}$$

In the particular cases of bosons $(\sigma_{\mathrm{F}}^{(\mathrm{b})})$ and of fermions $(\sigma_{\mathrm{F}}^{(\mathrm{f})})$, the above equation takes the forms

$$\sigma_{\mathrm{F}}^{(\mathrm{b})} = \frac{s+1}{2s+1}\sigma_+ + \frac{s}{2s+1}\sigma_-,$$

$$\sigma_{\mathrm{F}}^{(\mathrm{f})} = \frac{s}{2s+1}\sigma_+ + \frac{s+1}{2s+1}\sigma_-.$$

The above equations have a simple interpretation: $\sigma_{\mathrm{F}}^{(\mathrm{b})}$ and $\sigma_{\mathrm{F}}^{(\mathrm{f})}$ are weighted averages of the cross sections for even (σ_+) and odd (σ_-) parities, in collisions of bosons and fermions, respectively. In each case, the factors multiplying σ_+ and σ_- are the probabilities that the incident wave have an even or an odd parity. The exchange symmetry of the total quantum state is the product of the symmetry in spin space with the parity of the wave function in coordinate space. In this way, the symmetry of the spin state determines unambiguously the parity. Therefore, the statistical weights are given by the fraction of the $|S\nu\rangle$ states that have each symmetry in the spin space. This symmetry is determined by the Clebsch–Gordan coefficients [see Eq. (6)]. That is, states with even S are symmetric whereas states with odd S are antisymmetric. In this way, the fusion cross sections for bosons and for fermions can be written as

$$\sigma_{\mathrm{F}}^{(\mathrm{b})} = P_{\mathrm{S}}\sigma_+ + P_{\mathrm{A}}\sigma_-, \quad \sigma_{\mathrm{F}}^{(\mathrm{f})} = P_{\mathrm{A}}\sigma_+ + P_{\mathrm{S}}\sigma_-, \tag{A9}$$

with

$$P_{\mathrm{S}} = \frac{N_+}{N} \quad \text{and } P_{\mathrm{A}} = \frac{N_-}{N}, \tag{A10}$$

where $N = (2s+1)^2$ is the total number os spin states.

APPENDIX B: ANALYTICAL EVALUATION OF I_n

In this Appendix we present the details of the derivation of Eqs. (72) and (73).

We have to evaluate the integral

$$I_n = \int_0^\infty d\lambda \frac{G(\lambda)}{F(\lambda)}, \tag{B1}$$

where

$$G(\lambda) = \lambda e^{in\pi\lambda} \tag{B2}$$

and

$$F(\lambda) \equiv \frac{1}{T(\lambda, E)} = 1 + \exp\left[\alpha\left(\lambda^2 - \lambda_g^2\right)\right], \tag{B3}$$

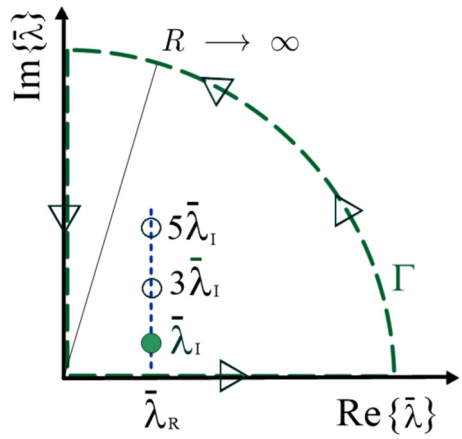

FIG. 10. The contour Γ used in evaluation of the integral of Eq. (B1). The three poles of the integrand closest to the real axis are represented by circles. Only the contribution from the pole with smallest imaginary part (green solid circle) is taken into account. Contributions for other poles (open circles) are neglected.

with

$$\alpha = \frac{\pi\hbar^2}{\mu\hbar\omega_{\rm E}R_{\rm E}^2}. \tag{B4}$$

To evaluate Eq. (B1), we perform the integration over the complex plane in a closed contour Γ, represented in Fig. 10. It is formed by the positive parts of the real and the imaginary axes, closing with a quadrant of a circumference of infinite radius. The result is given in terms of the residues of the poles of $F(\lambda)$ inside the circuit. Keeping only the contribution from the pole closest to the real axis, $\bar{\lambda}$, one gets

$$I_\Gamma \simeq 2\pi i \mathrm{Res}(\bar{\lambda}) \equiv 2\pi i \lim_{\lambda\to\bar{\lambda}} \left\{(\lambda-\bar{\lambda})\frac{G(\lambda)}{F(\lambda)}\right\}. \tag{B5}$$

The first step is to determine $\bar{\lambda}$. This pole is given by the condition

$$\exp\left[\alpha\left(\bar{\lambda}^2-\lambda_g^2\right)\right] = -1 \Longrightarrow \alpha\left(\bar{\lambda}^2-\lambda_g^2\right) = i\pi, \tag{B6}$$

where λ_g is the grazing angular momentum of Eq. (68). Writing the complex poles as $\bar{\lambda} = \lambda_{\rm R} + i\lambda_{\rm I}$, Eq. (B6) corresponds to the conditions

$$\lambda_{\rm I}^2 = \lambda_{\rm R}^2 - \lambda_g^2, \tag{B7}$$

$$\lambda_{\rm R}\lambda_{\rm I} = \frac{\pi}{2\alpha}. \tag{B8}$$

Using Eq. (B8) in Eq. (B7), one gets the equation

$$\lambda_{\rm R}^2 - \lambda_g^2 - \frac{\pi^2}{4\alpha^2\lambda_{\rm R}^2} = 0 \Longrightarrow \lambda_{\rm R}^4 - \lambda_g^2\lambda_{\rm R}^2 - \frac{\pi^2}{4\alpha^2} = 0, \tag{B9}$$

which has the solution

$$\lambda_{\rm R} = \frac{1}{\sqrt{2}}\left[\lambda_g^2 + \sqrt{\lambda_g^4 + \frac{\pi^2}{\alpha^2}}\right]^{1/2}. \tag{B10}$$

The imaginary part of the pole is given by Eq. (B8) as

$$\lambda_{\rm I} = \frac{\pi}{2\alpha\lambda_{\rm R}} = \frac{\mu\hbar\omega_{\rm E}R_{\rm E}^2}{2\hbar^2\lambda_{\rm R}}. \tag{B11}$$

We remark that, for high enough energies; that is, for $(E - V_{\rm E}) \gg \hbar\omega_{\rm E}/2$, one can approximate

$$\lambda_{\rm R} \simeq \lambda_g, \tag{B12}$$

$$\lambda_{\rm I} \simeq \frac{\mu\hbar\omega_{\rm E}R_{\rm E}^2}{2\hbar^2\lambda_g}. \tag{B13}$$

However, at lower energies these approximations break down. In the limit $E \to V_{\rm B}$, the grazing angular momentum vanishes. Then Eq. (B13) diverges, whereas Eq. (B11) tends to the finite limit

$$\lambda_{\rm I} = \frac{R_{\rm E}}{\hbar}\sqrt{\mu\hbar\omega_{\rm E}}.$$

According to Rowley and Hagino [16], the integral along the circumference of infinite radius vanishes, and the integral along the imaginary axis is negligible. Thus, one can approximate, $I_\Gamma \simeq I_n$. The integral I_n can then be evaluated by Eq. (B5). Expanding $F(\lambda)$ around $\bar{\lambda}$ and inserting the expansion into Eq. (B5), one gets

$$I_n(E) = 2\pi i \frac{G(\bar{\lambda})}{F'(\bar{\lambda})}, \tag{B14}$$

where $F'(\bar{\lambda})$ is the first derivative of $F(\lambda)$ at $\lambda = \bar{\lambda}$, which has the value

$$F'(\bar{\lambda}) = -2\alpha\bar{\lambda}. \tag{B15}$$

Using the explicit forms of $G(\lambda)$ and α, we get for $|n| \neq 0$,

$$I_n(E) = -i\frac{\mu\hbar\omega_{\rm E}R_{\rm E}^2}{\hbar^2}e^{-n\pi\lambda_{\rm I}}e^{in\pi\lambda_{\rm R}}. \tag{B16}$$

Now we calculate $\Delta\sigma_0(E)$ and $\sigma_{\rm osc}$. We start from Eq. (58),

$$\Delta\sigma_0(E) = -\frac{4\pi}{k^2}\mathrm{Re}\{I_2(E)\},$$

and use Eq. (B16) for $n = 2$. We get

$$\Delta\sigma_0(E) = \frac{4\pi}{k^2}\frac{\mu\hbar\omega_{\rm E}R_{\rm E}^2}{\hbar^2}e^{-2\pi\lambda_{\rm I}}\,\mathrm{Re}\{ie^{i2\pi\lambda_{\rm R}}\}. \tag{B17}$$

Taking the real part of $iI_2(E)$ and writing k^2 in terms of the collision energy, one obtains

$$\Delta\sigma_0(E) = -2\pi\frac{\hbar\omega_{\rm E}}{E}R_{\rm E}^2e^{-2\pi\lambda_{\rm I}}\,\sin(2\pi\lambda_{\rm R}), \tag{B18}$$

or, replacing $\lambda_{\rm R} = l_{\rm R} + 1/2$ and using the relation

$$\sin(2\pi\lambda_{\rm R}) = \sin[2\pi(l_{\rm R}+1/2)] = -\sin(2\pi l_{\rm R}),$$

Eq. (B18) becomes

$$\Delta\sigma_0(E) = 2\pi\frac{\hbar\omega_{\rm E}}{E}R_{\rm E}^2e^{-2\xi}\,\sin(2\pi l_{\rm R}), \tag{B19}$$

with

$$\xi = \pi \frac{\mu \hbar \omega_{\rm E} R_{\rm E}^2}{2\hbar^2 \lambda_{\rm R}}. \tag{B20}$$

If the collision energy is not to close to $V_{\rm B}$, $\lambda_{\rm R}$ can be replaced by λ_g and one gets Eq. (71).

Now we evaluate $\sigma_{\rm osc}$. For this purpose, we insert Eq. (B16) for $n = 1$ into the expression [see Eq. (64)],

$$\sigma_{\rm osc}(E) = \frac{(-)^{2s}}{2s+1} \frac{4\pi}{k^2} {\rm Im}\{I_1(E)\}.$$

We get

$$\sigma_{\rm osc}(E) = -\frac{(-)^{2s}}{2s+1} 2\pi \frac{\hbar\omega_{\rm E}}{E} R_{\rm E}^2 e^{-\pi\lambda_{\rm I}} {\rm Re}\{e^{i\pi\lambda_{\rm R}}\}, \tag{B21}$$

or

$$\sigma_{\rm osc}(E) = -\frac{(-)^{2s}}{2s+1} 2\pi \frac{\hbar\omega_{\rm E}}{E} R_{\rm E}^2 e^{-\pi\lambda_{\rm I}} \cos(\pi\lambda_{\rm R}). \tag{B22}$$

Using the relation

$$\cos(\pi\lambda_{\rm R}) = \cos[\pi(l_{\rm R} + 1/2)] = -\sin(\pi l_{\rm R}),$$

the above equation becomes,

$$\sigma_{\rm osc}(E) = \frac{(-)^{2s}}{2s+1} 2\pi \frac{\hbar\omega_{\rm E}}{E} R_{\rm E}^2 e^{-\pi\lambda_{\rm I}} \sin(\pi l_{\rm R}). \tag{B23}$$

Except for the spin factor $(-)^{2s}/(2s+1)$ and the use of λ_R and λ_I, Eqs. (B19) and (B23) and the damping parameter, Eq. (B20), are the same as the corresponding ones obtained in Ref. [16].

[1] L. F. Canto, R. Donangelo, and M. S. Hussein, Mod. Phys. Lett. A **16**, 1027 (2001).
[2] L. F. Canto, M. S. Hussein, and W. Mittig, Phys. Rev. C **89**, 024610 (2014).
[3] M. N. A. Abdullah, M. S. Sabra, M. M. Rashid, Z. Shehadeh, M. M. Billah, S. K. Das, M. A. Uddin, A. K. Basak, I. Reichstein, H. M. Sen Gupta *et al.*, Nucl. Phys. A **775**, 1 (2006).
[4] D. M. Brink and G. R. Satchler, *Angular Momentum*, 3rd ed. (Clarendon Press, 1994).
[5] C. J. Joachain, *Quantum Collision Theory* (North Holland, 1983).
[6] O. Akyüz and A. Winther, in *Nuclear Structure of Heavy Ion Reactions*, edited by R. A. Broglia, C. H. Dasso, and R. A. Ricci (North Holland, 1981).
[7] R. A. Broglia and A. Winther, *Heavy Ion Reactions* (Westview Press, 2004).
[8] G. R. Satchler and W. G. Love, Phys. Rep. **55**, 183 (1979).
[9] L. F. Canto and M. S. Hussein, *Scattering Theory of Molecules, Atoms and Nuclei* (World Scientific Publishing Co. Pte. Ltd., 2013).
[10] L. R. Gasques, L. C. Chamon, P. R. S. Gomes, and J. Lubian, Nucl. Phys. A **764**, 135 (2006).
[11] G. Gruber, I. C. Dormehl, K. Meier-Ewert, and K. Bethege, Eur. Phys. J. A **265**, 411 (1973).
[12] H. T. Fortune, G. C. Morrison, and R. H. Siemssen, Phys. Rev. C **3**, 2133 (1971).
[13] G. Dietl, G. Gruber, H. Schmidt-Böcking, and K. Bethge, Nucl. Phys. A **250**, 322 (1975).
[14] D. L. Hill and J. A. Wheeler, Phys. Rev. **89**, 1102 (1953).
[15] C. Y. Wong, Phys. Rev. Lett. **31**, 766 (1973).
[16] N. Rowley and K. Hagino, Phys. Rev. C **91**, 044617 (2015).
[17] D. G. Kovar, D. F. Geesaman, T. H. Braid, Y. Eisen, W. Henning, T. R. Ophel, M. Paul, K. E. Rehm, S. J. Sanders, P. Sperr *et al.*, Phys. Rev. C **20**, 1305 (1979).
[18] L. F. Canto, P. R. S. Gomes, J. Lubian, L. C. Chamon, and E. Crema, J. Phys. G **36**, 015109 (2009).
[19] L. F. Canto, P. R. S. Gomes, J. Lubian, L. C. Chamon, and E. Crema, Nucl. Phys. A **821**, 51 (2009).
[20] L. F. Canto, D. R. Mendes Junior, P. R. S. Gomes, and J. Lubian, Phys. Rev. C **92**, 014626 (2015).